Thermoelectric transport in the coupled valence-band model

Ashok T. Ramu,[1,a)] Laura E. Cassels,[2] Nathan H. Hackman,[1] Hong Lu,[3] Joshua M. O. Zide,[2] and John E. Bowers[1]
[1]*Department of Electrical and Computer Engineering, University of California–Santa Barbara, Santa Barbara, California 93106, USA*
[2]*Department of Materials Science and Engineering, University of Delaware, 201 Dupont Hall, Newark, Delaware 19716, USA*
[3]*Department of Materials, University of California–Santa Barbara, Santa Barbara, California 93106, USA*

(Received 14 October 2010; accepted 4 December 2010; published online 1 February 2011)

The Boltzmann transport equation (BTE) is applied to the problem of thermoelectric transport in p-type semiconductors whose valence band-structure is describable in terms of two bands degenerate at the Γ point. The Seebeck coefficient and mobility are calculated from the solution to two coupled BTEs, one for each band, with interband scattering and scattering by inelastic mechanisms treated exactly by the application of an algorithm developed by the authors in an earlier work. Most treatments of this problem decouple the two bands by neglecting certain terms in the BTE, greatly simplifying the mathematics: the error in the Seebeck coefficient and mobility introduced by this approximation is quantified by comparing with the exact solution. Degenerate statistics has been assumed throughout, and the resulting formalism is therefore valid at high hole concentrations. Material parameters are used that have been deduced from optical, strain and other experiments often not directly related to hole transport. The formulations in this work thus do not use adjustable or fitting parameters. The transport coefficients of heavily doped gallium antimonide, a typical high-efficiency p-type thermoelectric material, are calculated and agreement to experimentally determined values is found to be satisfactory. © *2011 American Institute of Physics*. [doi:10.1063/1.3537826]

I. INTRODUCTION

The theory of thermoelectric transport in n-type III–V compound semiconductors is well understood, including the effects of inelastic scattering,[1–3] primarily due to the simplicity afforded by the fact that the conduction band-structure in these materials is often described to a very good approximation by the single spherical nonparabolic model.[4] However the treatment of transport in p-type materials is complicated mainly by following two factors: (a) the warping of constant-energy surfaces of the valence bands, especially the heavy-hole band, and (b) the interaction of the heavy-hole and light-hole bands (especially interactions mediated by optical-mode phonons), with the energy distribution of carriers in one influenced by that in the other. In particular, there is little information on the effect of optical-mode phonon scattering on the Seebeck coefficient, especially regarding the magnitudes of terms which cannot be treated under the relaxation time approximation.

In some cases, approximations have been made that considerably simplify the problem, while lending insight into the key physical processes. These include the assumption of a single relaxation time for both light and heavy holes, making it possible to decouple the bands.[5] However any accurate modeling of hole transport must include detailed descriptions of scattering due to each of several contributing scattering mechanisms.

Kranzer in his review article[6] has treated the problem of hole mobility of various III–V and II–VI compound semiconductors, solving the Boltzmann transport equation (BTE) exactly in two *k*-space coordinates. Kranzer assumes a spherical parabolic model for both bands; while this model is strictly not correct, the effect of band-warping is taken into account by postulating two effective masses for each band, one of which describes the density-of-states, thus entering the expressions for scattering rates, while the other describes the group velocity, thus entering expressions for the current. One of the limitations of Ref. 6 as applied to the problem under study is the nondegenerate approximation to the BTE: however this is not a serious limitation and it is only slightly more cumbersome to treat the full BTE. Reference 7 presents hole mobility calculations with intraband optical-mode phonon scattering treated exactly using a variational approach; however interband scattering is still treated under the relaxation time approximation.

In this work, we generalize the difference equation method described by Kranzer to the solution of the BTE in the presence of spatial fluctuations, such as necessary for the calculation of the Seebeck coefficient. A spherical parabolic model is assumed for both bands with band-warping partially accounted for through the use of two different but related effective masses for each band.[6,8] All intraband and interband scattering terms are taken into account, including those due to optical-mode phonons.

In Sec. II we state mathematically the form of the BTE in the coupled valence band model, and simplify the collision term to a more tractable form, from which mobility can be immediately derived. Section III describes the algorithm used to calculate the Seebeck coefficient from this formula-

a)Electronic mail: ashok.ramu@gmail.com.

tion. Next we describe the band-structure model used (Sec. IV), and calculate numerically the density-of-states effective mass and conductivity effective masses from the Luttinger–Kohn[9] model for the valence band-structure. In order to minimize the computational burden, Sec. V derives closed form expressions for scattering integrals (defined in Sec. II) due to all scattering mechanisms considered in this study. Section VI compares the results of the calculation to experimental Seebeck coefficient and mobility data on p-GaSb, a high efficiency thermoelectric material. Section VII summarizes our results.

II. THE TWO COUPLED BTES

The BTE is an integral-differential equation for the nonequilibrium distribution function in three k-space and three real-space coordinates. Throughout, bold font will be used for vectors, and normal font for their magnitudes and all other scalars. Also the subscripts i, j will refer to the heavy-hole and light-hole bands unless otherwise stated. The BTE for band i (heavy-hole band) is given by

$$\begin{aligned}\boldsymbol{v_i}(\boldsymbol{k_i})\cdot\boldsymbol{\nabla_r} f_i + \frac{q\boldsymbol{F}}{\hbar}\cdot\boldsymbol{\nabla_{k_i}} f_i \\ = \sum_{\boldsymbol{k_i'}} S_{ii}(\boldsymbol{k_i'},\boldsymbol{k_i}) f_i(\boldsymbol{k_i'},\boldsymbol{r})[1-f_i(\boldsymbol{k_i},\boldsymbol{r})] - \sum_{\boldsymbol{k_i'}} S_{ii}(\boldsymbol{k_i},\boldsymbol{k_i'}) f_i(\boldsymbol{k_i},\boldsymbol{r}) \\ \times[1-f_i(\boldsymbol{k_i'},\boldsymbol{r})] + \sum_{\boldsymbol{k_j'}} S_{ji}(\boldsymbol{k_j'},\boldsymbol{k_i}) f_j(\boldsymbol{k_j'},\boldsymbol{r})[1-f_i(\boldsymbol{k_i},\boldsymbol{r})] \\ - \sum_{\boldsymbol{k_j'}} S_{ij}(\boldsymbol{k_i},\boldsymbol{k_j'}) f_i(\boldsymbol{k_i},\boldsymbol{r})[1-f_j(\boldsymbol{k_j'},\boldsymbol{r})]. \end{aligned} \tag{1}$$

An analogous BTE can be written for the light-hole band by interchanging i and j in Eq. (1). The quantities $f_n(\boldsymbol{k_n},\boldsymbol{r}), n=i,j$ are the nonequilibrium distribution functions for the heavy-hole and the light-hole band, respectively. From these distribution functions, all bulk transport properties like the particle concentration, particle current, energy current, etc., in each band can be derived as a function of spatial coordinate $\boldsymbol{r}$, by taking the appropriate moment and integrating over all $\boldsymbol{k_n}$. Here the quantities $S_{mn}(\boldsymbol{k_m},\boldsymbol{k_n})$ represent the sum of transition probabilities per unit time due to all mechanisms, from a state with wave-vector $\boldsymbol{k_m}$ in the band "m," to a state of wave-vector $\boldsymbol{k_n}$ in band "n," where "m" and "n" can each take either of two values, i or j. Also $\boldsymbol{v_n}(\boldsymbol{k_n})$ is the group velocity in the band "n" and $\boldsymbol{F}(\boldsymbol{r})$ is the electric field at any point $\boldsymbol{r}$. The first two summations on the RHS of Eq. (1) represent intraband scattering, and the next two, interband scattering.

We assume that (a) variations in potential and temperature are along only one spatial direction, the z-direction, (b) the dispersion relation is spherically symmetric, (c) scattering rates depend only on the magnitudes of, and the angle between, the initial and final wave-vectors, and not on their absolute orientations, and (d) the two distribution functions $f_n, n=i,j$ possess azimuthal symmetry about the z-axis. Thus they can be expanded in a basis of spherical harmonics, and for low fields the expansion can be truncated to a single term (Ref. 2, p. 1015) as follows:

$$\begin{aligned} f_n(k_n,\theta_n,z) &= f_{0n}(k_n,z) + \sum_{l=1}^{\infty} g_{ln}(k_n,z) P_l(\cos\theta_n) \\ &\sim f_{0n}(k_n,z) + g_n(k_n,z)\cos\theta_n, \quad n=i,j. \end{aligned} \tag{2}$$

Here θ_n is the angle made with the z-axis by vector $\boldsymbol{k_n}$ of magnitude k_n. The symmetric part of the distribution function $f_{0n}(k_n,z)$, is given by Fermi–Dirac statistics, assumed unchanged by the applied electrothermal fields, $f_{0n}(k_n,z) = 1/[\exp[-E_n(k_n)-E_v(z)+E_F(z)]/k_BT(z)+1]$, where $E_n(k_n)$ is the dispersion relation for the hole band "n," $E_v(z)$ is the valence band profile, $E_F(z)$ is the chemical potential profile and $T(z)$ is the applied temperature profile. The profiles $E_v(z)$, $E_F(z)$, and $T(z)$ are inputs to the BTE solver, with their correct values determined by starting with an initial guess and iterating until charge neutrality and current continuity are simultaneously satisfied. An algorithm for the determination of these profiles is the subject of Sec. III. $g_n(k_n,z)$ is the unknown, antisymmetric part of the distribution function that gives rise to a net particle flux; the rest of this section deals with its determination. Henceforth, the term "distribution function" without any qualifier will refer to the antisymmetric part $g_n(k_n,z)$.

Let v_n be the magnitude of the group velocity in band "n." Due to assumption (b) above, it depends only on the magnitude k_n. $F(z)=dE_V(z)/dz$ is the electric field profile. For convenience, we classify scattering mechanisms as elastic and inelastic. $S^{\text{elas}}_{m,n}(\boldsymbol{k_m},\boldsymbol{k_n})$ is defined as the sum of transition probabilities per unit time due to elastic mechanisms from state $\boldsymbol{k_m}$ in band "m," into state $\boldsymbol{k_n}$ in band "n." For inelastic mechanisms, $S^{\text{inelas}}_{m,n}(\boldsymbol{k_m},\boldsymbol{k_n})$ is defined similarly. In general for inelastic mechanisms, $S^{\text{inelas}}_{m,n}(\boldsymbol{k_m},\boldsymbol{k_n}) \neq S^{\text{inelas}}_{n,m}(\boldsymbol{k_n},\boldsymbol{k_m})$. For example, for optical-mode phonon scattering, if one of the two quantities corresponds to phonon absorption, the other will correspond to phonon emission (Ref. 10, pp. 76–79).

Upon inserting Eq. (2) into Eq. (1), multiplying throughout by $\sin\theta_i\cos\theta_i d\theta_i$ and integrating with respect to θ_i the hole-band BTE reduces, in a straightforward extension of the derivation in the Appendix, Ref. 3, to

$$\begin{aligned} g_i(k_i,z)\left[\frac{1}{\tau_{i-\text{eff}}(k_i,z)}\right] = -\left[v_i(k_i)\left(\frac{\partial f_{0i}}{\partial z}\right) + \frac{qF(z)}{\hbar}\left(\frac{\partial f_{0i}}{\partial k_i}\right)\right] \\ + \int_{k_i'=0}^{\infty} \frac{g_i(k_i',z)}{\Gamma^{\text{inelas}}_{ii}(k_i',k_i,z)} dk_i' \\ + \int_{k_j'=0}^{\infty} \frac{g_j(k_j',z)}{\Gamma_{ji}(k_j',k_i,z)} dk_j', \end{aligned} \tag{3a}$$

$$\frac{1}{\tau_{i-\text{eff}}(k_i,z)} = \left(\frac{1}{\tau^{\text{inelas}}_{ii}(k_i,z)} + \frac{1}{\tau^{\text{elas}}_{ii-\text{mom}}(k_i)}\right) + \frac{1}{\tau_{ij}(k_i,z)}. \tag{3b}$$

The various terms in the Eqs. (3a) and (3b) are defined as follows:

$$\frac{1}{\tau_{ii}^{\text{inelas}}(k_i,z)} = \frac{1}{(2\pi)^3}\int\int\int_{k_i',\theta_i',\phi_i'} \{S_{ii}^{\text{inelas}}(\boldsymbol{k_i},\boldsymbol{k_i'})[1-f_{0i}(k_i',z)] + S_{ii}^{\text{inelas}}(\boldsymbol{k_i'},\boldsymbol{k_i})f_{0i}(k_i',z)\}d\Omega_i' k_i'^2 dk_i', \tag{4}$$

$$\frac{1}{\Gamma_{ii}^{\text{inelas}}(k_i',k_i,z)} = \left(\frac{3}{2}\right)\frac{1}{(2\pi)^3}\int_{\theta_i=0}^{\pi}\int\int_{\theta_i',\phi_i'} (S_{ii}^{\text{inelas}}(\boldsymbol{k_i'},\boldsymbol{k_i})[1-f_{0i}(k_i,z)] + S_{ii}^{\text{inelas}}(\boldsymbol{k_i},\boldsymbol{k_i'})f_{0i}(k_i,z))\cos\,\theta_i'\,\cos\,\theta_i\,\sin\,\theta_i d\theta_i k_i'^2 d\Omega_i'. \tag{5}$$

Equations (4) and (5) represent intraband scattering rates due to inelastic mechanisms, and roughly correspond to scattering out of, and scattering into, the state $\boldsymbol{k_i}$ respectively (Ref. 3, Eqs. A6 and A9),

$$\left(\frac{1}{\tau_{ii-\text{mom}}^{\text{elas}}(k_i)}\right) = \frac{1}{(2\pi)^3}\int\int\int_{k_i',\alpha_i,\gamma_i} S_{ii}^{\text{elas}}(k_i,k_i',\alpha_i)(1-\cos\,\alpha_i)\sin\,\alpha_i \mathrm{d}\alpha_i \mathrm{d}\gamma_i k_i'^2 dk_i'. \tag{6}$$

Equation (6) shows that for elastic intraband scattering, the in- and out-scattering rates can be combined into a single "momentum" scattering rate (Ref. 5, Eq. 6.2.23). In order to bring it to a standard form (Ref. 10, Eq. 2.4), the integral over all final states is shown about $\boldsymbol{k_i}$ as the polar axis (instead of the z-axis), the polar angles being α_i, γ_i. The integral over k_i' in Eq. (6) is dummy, since $S_{ii}^{\text{elas}}(k_i,k_i',\alpha_i)$ for elastic mechanisms contains a factor $\delta[E_i(k_i)-E_i(k_i')]$.

$$\frac{1}{\tau_{ij}(k_i,z)} = \frac{1}{(2\pi)^3}\int\int\int_{k_j',\theta_j',\phi_j'} \{S_{ij}(\boldsymbol{k_i},\boldsymbol{k_j'})[1-f_{0j}(k_j',z)] + S_{ji}(\boldsymbol{k_j'},\boldsymbol{k_i})f_{0j}(k_j',z)\}d\Omega_j' k_j'^2 dk_j', \tag{7}$$

$$\frac{1}{\Gamma_{ji}(k_j',k_i,z)} = \left(\frac{3}{2}\right)\frac{1}{(2\pi)^3}\int_{\theta_i=0}^{\pi}\int\int_{\theta_j',\phi_j'} (S_{ji}(\boldsymbol{k_j'},\boldsymbol{k_i})[1-f_{0i}(k_i,z)] + S_{ij}(\boldsymbol{k_i},\boldsymbol{k_j'})f_{0i}(k_i,z))\cos\,\theta_j'\,\cos\,\theta_i\,\sin\,\theta_i d\theta_i k_j'^2 d\Omega_j'. \tag{8}$$

Equations (7) and (8) are interband scattering rates due to all mechanisms. For interband scattering, we make no notational distinction between elastic and inelastic mechanisms since there is no significant mathematical advantage such as that seen in Eq. (6). An equation similar to Eq. (3) can be written down for the light-hole band simply by interchanging i and j in Eq. (3) and in the definitions following it, Eqs. (4)–(8). In later sections, we derive expressions for the above terms for scattering due to each mechanism of interest.

Equation (3) illustrates the nature of the difficulty posed by the terms containing $1/\Gamma_{ii}^{\text{inelas}}$ and $1/\Gamma_{ji}$. As mentioned in the introduction, they cause the population of carriers at a given energy in a given band to depend on the population at a different energy in the same band, as well as on the distribution of carriers in the other band. The mobility calculation of Ref. 5, Chap. 8 ignores both these terms, that of Ref. 7 treats terms $1/\Gamma_{ii}^{\text{inelas}}$ but not $1/\Gamma_{ji}$, and that of Ref. 6 treats both but uses the nondegenerate form of the BTE.

We use numerical iteration[2] to solve the two equations, namely, Eq. (3) and the analogous one for the light-hole band. The M^{th} iterates for the heavy-hole band and the light-hole band distribution functions, $g_i^{(M)}(k_i,z)$ and $g_j^{(M)}(k_j,z)$ are given by the following recursion relations:

$$\begin{aligned} g_i^{(M)}(k_i,z) = &-\tau_{i-\text{eff}}(k_i,z)\left[v_i(k_i)\left(\frac{\partial f_{0i}}{\partial z}\right) + \frac{qF(z)}{\hbar}\left(\frac{\partial f_{0i}}{\partial k_i}\right)\right] \\ &+ \tau_{i-\text{eff}}(k_i,z)\int_{k_i'=0}^{\infty}\frac{g_i^{(M-1)}(k_i',z)}{\Gamma_{ii}^{\text{inelas}}(k_i',k_i,z)}dk_i' \\ &+ \tau_{i-\text{eff}}(k_i,z)\int_{k_j'=0}^{\infty}\frac{g_j^{(M-1)}(k_j',z)}{\Gamma_{ji}(k_j',k_i,z)}dk_j', \end{aligned} \tag{9a}$$

$$\begin{aligned} g_j^{(M)}(k_j,z) = &-\tau_{j-\text{eff}}(k_j,z)\left[v_j(k_j)\left(\frac{\partial f_{0j}}{\partial z}\right) + \frac{qF(z)}{\hbar}\left(\frac{\partial f_{0j}}{\partial k_j}\right)\right] \\ &+ \tau_{j-\text{eff}}(k_j,z)\int_{k_j'=0}^{\infty}\frac{g_j^{(M-1)}(k_j',z)}{\Gamma_{jj}^{\text{inelas}}(k_j',k_j,z)}dk_j' \\ &+ \tau_{j-\text{eff}}(k_j,z)\int_{k_i'=0}^{\infty}\frac{g_i^{(M-1)}(k_i',z)}{\Gamma_{ij}(k_i',k_j,z)}dk_i'. \end{aligned} \tag{9b}$$

The iteration is begun at $M=1$ by setting $g_i^{(0)}(k_i,z) = g_j^{(0)}(k_j,z) = 0$ on the right-hand side.

Once the two distribution functions are known, the current density at any point z is calculated using

$$J(z) = \left(\frac{q}{3\pi^2}\right)\left[\int_{k_i=0}^{\infty} k_i^2 v_i(k_i) g_i^{(M)}(k_i,z)dk_i + \int_{k_j=0}^{\infty} k_j^2 v_j(k_j) g_j^{(M)}(k_j,z)dk_j\right]. \tag{10}$$

This sum of the current contributions from the two bands is the output of the BTE solver. For the special case of spatially uniform electric fields, suppressing the spatial dependence in Eqs. (9) and (10) gives immediately the conductivity of each band. Starting iteration at $M=1$, with $g_i^{(0)}(k_i) = g_j^{(0)}(k_j) = 0$,

$$g_i^{(M)}(k_i) = -\tau_{i-\mathrm{eff}}(k_i)\frac{qF}{\hbar}\left(\frac{\partial f_{0i}}{\partial k_i}\right) + \tau_{i-\mathrm{eff}}(k_i)\int_{k_i'=0}^{\infty}\frac{g_i^{(M-1)}(k_i')}{\Gamma_{ii}^{\mathrm{inelas}}(k_i',k_i)}dk_i' + \tau_{i-\mathrm{eff}}(k_i)\int_{k_j'=0}^{\infty}\frac{g_j^{(M-1)}(k_j')}{\Gamma_{ji}(k_j',k_i)}dk_j', \tag{11a}$$

$$g_j^{(M)}(k_j) = -\tau_{j-\mathrm{eff}}(k_j)\frac{qF}{\hbar}\left(\frac{\partial f_{0j}}{\partial k_j}\right) + \tau_{j-\mathrm{eff}}(k_j)\int_{k_j'=0}^{\infty}\frac{g_j^{(M-1)}(k_j')}{\Gamma_{jj}^{\mathrm{inelas}}(k_j',k_j)}dk_j' + \tau_{j-\mathrm{eff}}(k_j)\int_{k_i'=0}^{\infty}\frac{g_i^{(M-1)}(k_i')}{\Gamma_{ij}(k_i',k_j)}dk_i', \tag{11b}$$

$$\sigma_n = \left(\frac{q}{3\pi^2 F}\right)\int_{k_n=0}^{\infty} k_n^2 v_n(k_n) g_n^{(M)}(k_n)dk_n, \quad n=i,j. \tag{12}$$

A few remarks are in order here about the iterative calculation of the distribution functions, Eqs. (9) and (11). First, it is seen that five iterations (up to $M=5$) are sufficient for convergence within 0.1% for mobility calculation. For example, in 4.5×10^{19} cm^{-3} p-GaSb at 600 K, the first few iterates of the mobility are 106.332, 123.342, 126.240, 126.742, 126.830, and 126.846 $\mathrm{cm}^2/\mathrm{V\,s}$. Second, if only elastic scattering mechanisms are considered, the pair of Eqs. (9a) and (9b) can be solved exactly without numerical iteration by change of coordinates to energy instead of k since we get a pair of simultaneous equations at each value of energy.[11] However since we treat inelastic mechanisms as well in this work, there is no advantage in switching to energy coordinates. Third, using a noniterative approximation to the distribution functions, i.e., setting $M=1$ in Eqs. (9a) and (9b) results in a very simple expression for the Seebeck coefficient, and this is stated in Sec. VI, Eqs. (31a)–(31c) following a discussion of the accuracy of this approximation.

III. ALGORITHM FOR EXTRACTION OF THE SEEBECK COEFFICIENT

In order to determine the Seebeck coefficient from Eqs. (9a), (9b), and (10), one end of a sample of length L is assumed kept at the temperature T (Kelvin) at which the Seebeck coefficient is sought, the other at $(T+\Delta)$ K. Although the following procedure for calculating thermoelectric voltages is valid for any arbitrary temperature difference Δ, the Seebeck coefficient is defined in the limit as Δ approaches 0. Thus we choose $\Delta<5$ for the calculations in this work. The temperature variation is assumed to be linear and chosen to lie along the z-axis. Close to equilibrium, space charge neutrality holds in the bulk of the device. Knowing $T(z)$ and the hole concentration as a function of T, the difference between the valence band edge profile and the chemical potential profile $[E_v(z)-E_F(z)]$ is determined using the relation

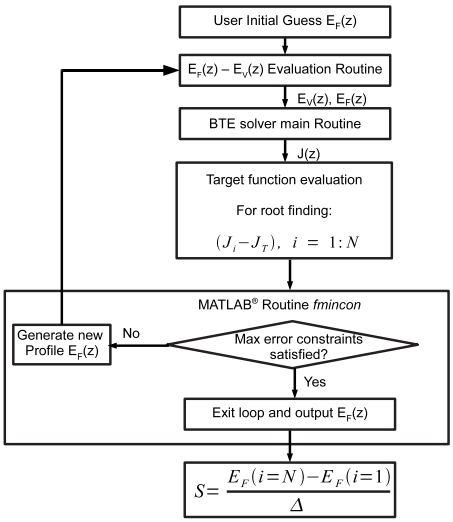

FIG. 1. Schematic of algorithm (Ref. 3) for calculation of the Seebeck coefficient.

$$p[T(z)] = \left(\frac{1}{\pi^2}\right)\sum_{n=i,j}\int_{k_n=0}^{\infty} \times \frac{k_n^2 dk_n}{1+\exp\left[\dfrac{(\hbar^2k_n^2/2m_n^{\mathrm{DOS}}) - E_v(z) + E_F(z)}{k_B T(z)}\right]}. \tag{13}$$

Above, m_n^{DOS} is the density-of-states effective mass (see Sec. IV) of band "n." The hole concentration p is practically independent of T over the small range T to $(T+\Delta)$.

Assuming a spatial grid of N points, the current profile can be discretized into a vector $[J_1, J_2 J_3, \ldots, J_N]$, and the chemical potential profile into a vector $[E_{F1}, E_{F2}, E_{F3}, \ldots, E_{FN}]$. The problem of imposing current continuity is equivalent to finding the roots of an N-dimensional equation $f([E_{F1}, E_{F2}, \ldots, E_{FN}])=[J_1-J_T, J_2-J_T, \ldots, J_N-J_T]=[0]$. For Seebeck coefficient calculation the target current $J_T=0$. In this work, root-finding is done numerically using the MATLAB® nonlinear optimization routine "*fmincon*," which iteratively solves general constrained optimization problems. "fmincon" generates successive guesses for the chemical potential profile $E_F(z)$ and eventually the correct profile that satisfies $f([E_{F1}, E_{F2}, \ldots, E_{FN}])=[0]$. In practice, for doping concentrations of the order 10^{19} cm^{-3}, the numerical solver achieves a final current density of $\sim10^{-4}$ $\mathrm{A/m}^2$. Finally, the Seebeck coefficient is the difference between the chemical potentials at the two ends divided by Δ, the temperature difference. Figure 1 shows a schematic of this algoithm, modified from Fig. 3 of Ref. 3.

IV. BAND-STRUCTURE MODEL: DENSITY-OF-STATES AND CONDUCTIVITY EFFECTIVE MASSES

The warping of the constant energy surfaces of the valence bands of III–Vs, especially the heavy-hole band, introduces a large scatter in values of effective masses measured by various techniques. For example, values of the density-of-states effective mass of GaSb quoted in the literature range

from $0.36m_0$ (Ref. 6) to as large as $0.82m_0$.[12] Our approach in this work is to extract both the density-of-states and conductivity effective masses from the three Luttinger parameters of the material, and then use the recommendations of Vurgaftman *et al.*, Ref. 13, for the values of these parameters for a specific material.

For an arbitrary dispersion relation, the number of states $N_n(E_{\mathrm{Max}})$ per unit volume bounded by the surface of constant energy $E_{\mathrm{Max}}<0$ below the valence band-edge is given by a change of variables from the set (k_n,θ_n,ϕ_n) to (E_n,θ_n,ϕ_n). The Jacobian of the transformation[14] is $(\partial k_n/\partial E_n)$, giving

$$N_n(E_{\mathrm{Max}}) = (1/4\pi^3)\int\int\int_{E_n=0,\ \theta_n=0,\ \phi_n=0}^{E_n=E_{\mathrm{Max}},\ \theta_n=\pi,\ \phi_n=2\pi} (\partial k_n/\partial E_n) \times [k_n(E_n,\theta_n,\phi_n)]^2 dE_n d\Omega_n \quad n=i,j, \tag{14}$$

where $d\Omega_n$ is the infinitesimal solid angle.

We use the dispersion relation of Luttinger and Kohn,[9] referred to hereafter as the LK model. Except very close to $k=0$ where k-linear terms in the Hamiltonian are significant, we have for the hole spectrum,

$$E(\boldsymbol{k}) = -Ak^2 \pm \sqrt{B^2k^4 + C^2(k_x^2k_y^2 + k_y^2k_z^2 + k_z^2k_x^2)}. \tag{15}$$

The upper sign is for the heavy-hole band, and the lower is for the light-hole band. Constants A, B, and C of the LK model can be related[15] to the standard Luttinger parameter set. The integrations in Eq. (14) were evaluated numerically using the MATLAB® routine *trapz*.

In a parabolic model, the number of states per unit volume up to energy E_{Max} equals

$$N_n(E_{\mathrm{Max}}) = \left(\frac{1}{4\pi^3}\right)\left(\frac{4\pi}{3}\right)\left(\frac{2m_n^{\mathrm{DOS}}|E_{\mathrm{Max}}|}{\hbar^2}\right)^{3/2}, \tag{16}$$

where m_n^{DOS} is the density-of-states effective mass of band "n." Equating Eqs. (14) and (16) one can extract m_n^{DOS} as a function of E_{Max}. The DOS effective masses of the heavy-hole and light-hole bands of GaSb obtained from this calculation are $0.459m_0$ and $0.041m_0$, m_0 being the rest mass of a free electron. These values show negligible dependence on E_{Max}. These values are consistent with the power-series expansion, Eq. 8.1.23 of Ref. 5, which gives $0.452m_0$ and $0.041m_0$ for the heavy-hole and light-hole bands respectively of GaSb.

We use the following procedure for numerical calculation of the conductivity effective mass. Only under the relaxation time approximation, equivalent to $M=1$ in Eqs. (11) and (12), there is an exact expression for conductivity (see Eq. 8.3.10, Ref. 5) that takes into account the full LK bandstructure, and this expression is rewritten below

$$\sigma_n = \left(\frac{-q^2}{4\pi\hbar^2}\right)\int\int\int_{k_n,\theta_n,\phi_n} \tau_{n-\mathrm{eff}}(k_n) \times\left(\frac{\partial E_n}{\partial k_{nz}}\right)^2\left(\frac{\partial f_0}{\partial E_n}\right)k_n^2 dk_n \sin\theta_n d\theta_n d\phi_n, \quad n=i,j. \tag{17}$$

Here f_0 is the Fermi–Dirac function and k_{nz} is the z-component of the vector $\boldsymbol{k_n}$ at which the dispersion E_n is evaluated. The conductivity is now recalculated using $M=1$ in Eqs. (11) and (12). m_n^{Cond} enters through the defining relation $v_n(k_n)=\hbar k_n/m_n^{\mathrm{Cond}}$. Now m_n^{Cond} is adjusted until the two formulations (17), (11), and (12) give the same conductivity. Although the conductivities calculated using both Eqs. (17), (11), and (12) depend on the carrier concentration through the Fermi–Dirac function f_0, the effective mass extracted by equating them should not, in order for the whole procedure (of simplification of the LK model into two effective masses per band) to be valid. This is in fact the case for GaSb with the values $m_i^{\mathrm{Cond}}=0.34m_0$ and $m_j^{\mathrm{Cond}}=0.041m_0$ giving an agreement to 0.1% between the two conductivity expressions, over the range of hole concentrations 4×10^{16} to 5×10^{19} cm^{-3}. These values are also consistent with the fourth-order power series expansion, Eq. (15) of Ref. 8 which gives $m_i^{\mathrm{Cond}}=0.324m_0$ and $m_j^{\mathrm{Cond}}=0.041m_0$.

V. EXPLICIT EXPRESSIONS FOR THE SCATTERING RATES

In this section, we state closed form expressions for all scattering terms defined by Eqs. (4)–(8) due to four scattering mechanisms: polar optical-mode phonon (POP) scattering, nonpolar optical-mode phonon (NPOP) scattering, screened ionized impurity (SII) scattering and acoustic-mode phonon deformation potential scattering. Throughout this section, masses m_i and m_j refer to the density-of-states effective masses of the two bands. Rates relevant to the heavy-hole band BTE only will be shown; interchanging labels i and j gives the corresponding rate expressions for the light-hole bands. Overlap integrals are included, which to a good approximation[16] depend only on the angle between the initial and final wave-vectors.

In what follows, ε_{r0} and $\varepsilon_{r\infty}$ are the static and high-frequency dielectric constants respectively and $\hbar\omega_{\mathrm{OP}}$ is the optical phonon energy. N_{OP} is the optical phonon occupation number, given by

$$N_{\mathrm{OP}} = \frac{1}{\exp\left(\frac{\hbar\omega_{\mathrm{OP}}}{k_BT}\right)-1}, \tag{18}$$

POP scattering is inelastic. Substituting in Eqs. (4) and (5) the interstate transition probability rate of Eq. (22), Ref. 6, and performing the required integration over all final states, we find,

$$\frac{1}{\tau_{ii}^{\mathrm{POP}}(k_i,z)} = \left(\frac{q^2\omega_{\mathrm{POP}}m_i}{16\pi\hbar^2k_i}\right)\left(\frac{1}{\varepsilon_{r\infty}}-\frac{1}{\varepsilon_{r0}}\right)((B^+)\{N_{\mathrm{OP}}[1-f_{0i}(k_i^+,z)]+(N_{\mathrm{OP}}+1)f_{0i}(k_i^+,z)\}+(B^-)\{(N_{\mathrm{OP}}+1)[1-f_{0i}(k_i^-,z)] + (N_{\mathrm{OP}})f_{0i}(k_i^-,z)\}), \tag{19a}$$

$$B^{\pm}=\left(\frac{(1+3c_i^{\pm 2})}{2}\log\left|\frac{1+c_i^{\pm}}{1-c_i^{\pm}}\right|-3c_i^{\pm}\right),\quad c_i^{\pm}=\frac{k_i^2+k_i^{\pm 2}}{2k_ik_i^{\pm}},\tag{19b}$$

$$\int_{k_i'=0}^{\infty}\frac{g_i(k_i',z)}{\Gamma_{ii}^{\mathrm{POP}}(k_i',k_i,z)}dk_i'=\left(\frac{q^2\omega_{\mathrm{OP}}m_i}{16\pi\hbar^2k_i}\right)\left(\frac{1}{\varepsilon_{r\infty}}-\frac{1}{\varepsilon_{r0}}\right)(g_i(k_i^+,z)(C^+)\{(N_{\mathrm{OP}}+1)[1-f_{0i}(k_i,z)]+N_{\mathrm{OP}}f_{0i}(k_i,z)\}+g_i(k_i^-,z)(C^-)$$
$$\times\{N_{\mathrm{OP}}[1-f_{0i}(k_i,z)]+(N_{\mathrm{OP}}+1)f_{0i}(k_i,z)\}),\tag{20a}$$

$$C^{\pm}=\left\{\frac{(c_i^{\pm}+3c_i^{\pm 3})}{2}\log\left|\frac{1+c_i^{\pm}}{1-c_i^{\pm}}\right|-[2+3(c_i^{\pm})^2]\right\},\quad c_i^{\pm}=\frac{k_i^2+k_i^{\pm 2}}{2k_ik_i^{\pm}}.\tag{20b}$$

In Eqs. (19) and (20), $k_i^{\pm}$ is the solution to the equation $E_i(k_i^{\pm})=E_i(k_i)\pm\hbar\omega_{\mathrm{OP}}$ for each sign + or – respectively. POP interband scattering terms are calculated in the same way from Eqs. (7) and (8) as follows:

$$\frac{1}{\tau_{ij}^{\mathrm{POP}}(k_i,z)}=\left(\frac{3q^2\omega_{\mathrm{OP}}m_j}{16\pi\hbar^2k_i}\right)\left(\frac{1}{\varepsilon_{r\infty}}-\frac{1}{\varepsilon_{r0}}\right)((D^+)\{N_{\mathrm{OP}}[1-f_{0j}(k_{ij}^+,z)]+(N_{\mathrm{OP}}+1)f_{0j}(k_{ij}^+,z)\}+(D^-)\{(N_{\mathrm{OP}}+1)[1-f_{0j}(k_{ij}^-,z)]$$
$$+(N_{\mathrm{OP}})f_{0j}(k_{ij}^-,z)\}),\tag{21a}$$

$$D^{\pm}=\left(\frac{(1+-c_{ij}^{\pm 2})}{2}\log\left|\frac{1+c_{ij}^{\pm}}{1-c_{ij}^{\pm}}\right|+c_{ij}^{\pm}\right),\quad c_{ij}^{\pm}=\frac{k_i^2+k_{ij}^{\pm 2}}{2k_ik_{ij}^{\pm}},\tag{21b}$$

$$\int_{k_j'=0}^{\infty}\frac{g_j(k_j',z)}{\Gamma_{ji}^{\mathrm{POP}}(k_j',k_i,z)}dk_j'=\left(\frac{3q^2\omega_{\mathrm{OP}}m_j}{16\pi\hbar^2k_i}\right)\left(\frac{1}{\varepsilon_{r\infty}}-\frac{1}{\varepsilon_{r0}}\right)(g_j(k_{ij}^+,z)(E^+)\{(N_{\mathrm{OP}}+1)[1-f_{0i}(k_i,z)]+N_{\mathrm{OP}}f_{0i}(k_i,z)\}+g_j(k_{ij}^-,z)(E^-)$$
$$\times\{N_{\mathrm{OP}}[1-f_{0i}(k_i,z)]+(N_{\mathrm{OP}}+1)f_{0i}(k_i,z)\}),\tag{22a}$$

$$E^{\pm}=\left(\frac{(c_{ij}^{\pm}-c_{ij}^{\pm 3})}{2}\log\left|\frac{1+c_{ij}^{\pm}}{1-c_{ij}^{\pm}}\right|+\frac{(3(c_{ij}^{\pm})^2-2)}{3}\right),\quad c_{ij}^{\pm}=\frac{k_i^2+k_{ij}^{\pm 2}}{2k_ik_{ij}^{\pm}}.\tag{22b}$$

In Eqs. (21) and (22) $k_{ij}^{\pm}$ is the solution to the equation $E_j(k_{ij}^{\pm})=E_i(k_i)\pm\hbar\omega_{\mathrm{OP}}$.

The interstate transition probability rate for NPOP inelastic scattering is given by Eqs. 17(a)-(20) of Ref. 6 in terms of the constants E_{NPOP} and $\bar{c}$ defined therein. It is to be noted that the transition probability rate is independent of the angle between the initial and final states even after accounting for the p-like character of the valence bands[17] with the result that any scattering rate weighed by $\cos\theta_n'(n=i,j)$ is 0 as follows:

$$\frac{1}{\Gamma_{ii}^{\mathrm{NPOP}}(k_i',k_i,z)}=\frac{1}{\Gamma_{ji}^{\mathrm{NPOP}}(k_j',k_i,z)}=0.\tag{23}$$

The other relevant scattering rates are given by

$$\frac{1}{\tau_{ii}^{\mathrm{NPOP}}(k_i,z)}=\frac{E_{\mathrm{NPOP}}^2\omega_{\mathrm{OP}}m_ik_i^+}{2\pi\hbar^2\bar{c}}\{N_{\mathrm{OP}}[1-f_{0i}(k_i^+,z)]$$
$$+(N_{\mathrm{OP}}+1)f_{0i}(k_i^+,z)\}$$
$$+\frac{E_{\mathrm{NPOP}}^2\omega_{\mathrm{OP}}m_ik_i^-}{2\pi\hbar^2\bar{c}}\{(N_{\mathrm{OP}}+1)[1-f_{0i}(k_i^-,z)]$$
$$+(N_{\mathrm{OP}})f_{0i}(k_i^-,z)\},\tag{24}$$

$$\frac{1}{\tau_{ij}^{\mathrm{NPOP}}(k_i,z)}=\frac{E_{\mathrm{NPOP}}^2\omega_{\mathrm{OP}}m_jk_{ij}^+}{2\pi\hbar^2\bar{c}}(N_{\mathrm{OP}}[1-f_{0j}(k_{ij}^+,z)]$$
$$+(N_{\mathrm{OP}}+1)f_{0j}(k_{ij}^+,z))$$
$$+\frac{E_{\mathrm{NPOP}}^2\omega_{\mathrm{OP}}m_jk_{ij}^-}{2\pi\hbar^2\bar{c}}((N_{\mathrm{OP}}+1)[1-f_{0j}(k_{ij}^-,z)]$$
$$+(N_{\mathrm{OP}})f_{0j}(k_{ij}^-,z)).\tag{25}$$

As with intraband POP scattering, $k_i^{\pm}$ in Eq. (24) is the solution to the equation $E_i(k_i^{\pm})=E_i(k_i)\pm\hbar\omega_{\mathrm{OP}}$ and $k_{ij}^{\pm}$ in Eq. (25) is the solution to the equation $E_j(k_{ij}^{\pm})=E_i(k_i)\pm\hbar\omega_{\mathrm{OP}}$.

Scattering by SIIs is elastic. Let N_{imp} be the number of ionized impurities and λ_s be the inverse screening length. $\lambda^2=\lambda_{si}^2+\lambda_{sj}^2$; where λ_{sn}^2 for each individual band "n" is calculated using Eq. (3) of Ref. 18. The momentum scattering rate [see Eq. (6)] for intraband transitions is given by

$$\frac{1}{\tau_{ii-\mathrm{mom}}^{\mathrm{SII}}(k_i)}=\frac{q^4N_{\mathrm{imp}}m_i}{32\pi\varepsilon_{r0}^2\hbar^3k_i^3}\left|(3A-1)^2\log\left|\frac{A+1}{A-1}\right|-2\left(9A-6+\frac{4}{A+1}\right)\right|,\tag{26a}$$

$$A = \frac{1}{2}\left(2 + \frac{\lambda_s^2}{k_i^2}\right). \tag{26b}$$

Interband scattering rates for SIIs under the Born approximation are given by

$$\frac{1}{\tau_{ij}^{\mathrm{SII}}(k_i,z)} = \frac{3q^4 N_{\mathrm{imp}}\sqrt{m_i m_j}}{32\pi\varepsilon_{r0}^2\hbar^3 k_i^3}\left|2F\log\left|\frac{F+1}{F-1}\right| - 4\right|, \tag{27}$$

$$\int_{k_j'=0}^{\infty}\frac{g_j(k_j',z)}{\Gamma_{ji}^{\mathrm{SII}}(k_j',k_i,z)}dk_j' = \frac{3q^4 N_{\mathrm{imp}}\sqrt{m_i m_j}}{32\pi\varepsilon_{r0}^2\hbar^3 k_i^3}\left|(3F^2-1)\log\left|\frac{F+1}{F-1}\right| - 6F\right| g_j(k_{ij},z), \tag{28a}$$

$$F = \frac{1}{2}\left(\sqrt{\frac{m_i}{m_j}} + \sqrt{\frac{m_j}{m_i}}\right) + \left(\frac{\lambda_s^2}{2k_i^2}\right)\sqrt{\frac{m_i}{m_j}}, \tag{28b}$$

k_{ij} in Eqs. (28) solves $E_j(k_{ij})=E_i(k_i)$. The expressions (26)–(28) are identical to Eq. 49, Ref. 11, except for a factor of $\sqrt{m_i/m_j}$ in their third equation.

Acoustic-mode phonon deformational potential scattering is very nearly elastic, and contributes about 15% to the net scattering rate. An often used approximation due to Lawaetz[17] is to treat acoustic-mode phonon deformational potential scattering as momentum randomizing.

$$\frac{1}{\tau_{ii-\mathrm{mom}}^{\mathrm{ADP}}(k_i)} = \left(\frac{k_B T\Xi^2}{2\pi\hbar^3 c_l}\right) m_i k_i, \tag{29a}$$

$$\frac{1}{\tau_{ij}^{\mathrm{ADP}}(k_i)} = \left(\frac{k_B T\Xi^2}{2\pi\hbar^3 c_l}\right) m_j k_{ij}, \tag{29b}$$

$$\frac{1}{\Gamma_{ji}^{\mathrm{ADP}}(k_{ij},k_i,z)} = 0. \tag{29c}$$

Again k_{ij} in Eqs. (29) solves $E_j(k_{ij})=E_i(k_i)$. Equation (29c) follows from the momentum-randomizing assumption. The constants in Eqs. (29) are defined below, following Eq. 5.2 and 5.3 of Ref. 17 as follows:

$$\Xi^2 = \frac{1}{2}\left[a^2 + \left(\frac{c_l}{c_t}\right)\left(b^2 + \frac{d^2}{2}\right)\right], \tag{30a}$$

$$c_l = \frac{1}{5}(3c_{11} + 2c_{12} + 4c_{44}), \tag{30b}$$

$$c_t = \frac{1}{5}(c_{11} - c_{12} + 3c_{44}). \tag{30c}$$

The quantities c_{11}, c_{12}, and c_{44} are the usual elastic stiffness coefficients[19] for a cubic crystal and (a,b,d) are the valence band deformation potentials.[20]

VI. COMPARISON TO EXPERIMENT

The above calculations are performed on p-type GaSb. GaSb, InGaSb, and their erbium-based nanocomposites are promising materials for p-type thermoelectrics owing to their combination of higher hole mobilities and lower thermal conductivities compared to corresponding arsenides and nitrides. The various material parameters involved in the calculation for GaSb, and their sources are given below. m_0 is the free electron mass, ε_0 is the permittivity of free space.

1. General parameters:[21] lattice constant $a_0=6.096\times10^{-10}$ m, density $\rho=5.61\times10^3$ kg/m^3.
2. Parameters pertaining to NPOP scattering:[21] optical phonon energy $\hbar\omega_{\mathrm{OP}}=29.7$ meV, static dielectric constant $\varepsilon_{r0}=15.7\varepsilon_0$.
3. Parameters pertaining to POP scattering:[21] static dielectric constant $\varepsilon_{r0}=15.7\varepsilon_0$, high-frequency dielectric constant $\varepsilon_{r\infty}=14.4\varepsilon_0$.
4. Band structure parameters: band-gap[21] $E_g=0.726$ eV, Luttinger parameters[13] $\gamma_1=13.4$, $\gamma_2=4.7$, and $\gamma_3=6.0$.
5. Parameters pertaining to ADP scattering: Elastic constants[21] $C_{11}=0.883\times10^{11}$ N/m^2, $C_{12}=0.402\times10^{11}$ N/m^2, and $C_{14}=0.432\times10^{11}$ N/m^2. Valence band deformation potentials[13] $a=-0.8$ eV, $b=-2$ eV, and $d=-4.7$ eV.
6. Derived parameters [this work]: $E_{\mathrm{NPOP}}=7.462$ eV and $\bar{c}=0.584\times10^{11}$ N/m^2 (appear in expressions for NPOP scattering). Density of states effective masses: $0.459m_0$ for heavy-hole band and $0.041m_0$ for light-hole band. Conductivity effective masses: $0.340m_0$ for heavy-hole band and $0.041m_0$ for light-hole band.

The series of GaSb films used for this study was grown by molecular beam epitaxy on semi-insulating GaAs (100) substrates using solid source materials. Unintentionally doped (UID) GaSb has a high hole concentration, $\sim4\times10^{16}$ cm^{-3}, making it unsuitable as a substrate for thin-film electrical property measurements. Hence semi-insulating GaAs was chosen as the growth substrate. After the native oxide was desorbed from the GaAs surface, a 200 nm undoped GaAs buffer layer was grown. Following the arsenide to antimonide interface adjustment, a 50 nm UID GaSb buffer layer was grown to relieve the ~7.8% lattice mismatch between the GaSb and the GaAs. This was followed by growth of the actual film, 1 μm GaSb. The growth temperature was 530 °C for GaSb and the growth rate was 1 μm/h. Dopants such as beryllium and carbon were used to dope the GaSb films p-type, with hole concentrations ranging from 1.4×10^{17} to 4.5×10^{19} cm^{-3}. Figure 2 shows a summary of Hall effect measurements on this series of films.

Two independently controlled Peltier modules provide temperature differences for Seebeck coefficient measurements. A bar-shaped sample with Indium contacts straddles the two Peltier elements, with Wakefield® thermal compound used for good thermal contact between the elements and the sample. Temperature is measured using two type-K thermocouples in intimate contact with the semiconductor surface.

Hall Effect measurements were made on a standard square Van der Pauw geometry, with Ohmic contacts made to the GaSb thin film by electron-beam evaporation-deposition of the following metal stack: Ti/Au, 40/400 nm.[22] I-V sweeps showed that Ohmic contacts were established. To prevent the film from becoming shorted accidentally, the GaSb thin film

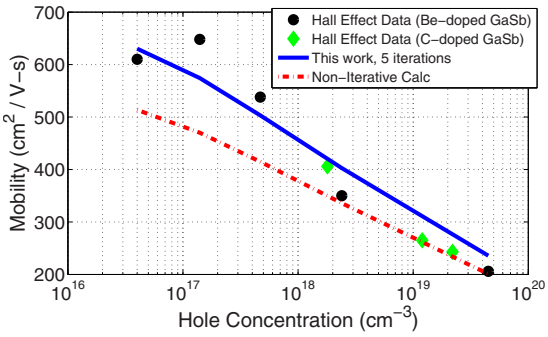

FIG. 2. (Color online) Room temperature mobility vs hole concentration, GaSb series (please see text for details about this series).

is etched away around the edges of the sample by Cl_2/Ar_2 based reactive ion etching (Ref. 23) leaving behind bare insulating substrate in those regions.

Figure 2 shows the room temperature mobility as extracted from Hall effect data, as a function of hole concentration. The mobility values extracted from Eqs. (11) and (12) with $M=5$ iterations are also plotted, as well as the result of the noniterative calculation ($M=1$). The improvement of accuracy afforded by the iterative calculation is evident in the doping range below 10^{18} cm^{-3}, although the comparison is complicated by the Hall factor. The hole mobility is overestimated at high doping levels, consistent with the findings of Ref. 11 on the accuracy of the Born approximation. Nevertheless, our calculations agree with the experimental mobility to within 20% over three decades in hole concentration. Additionally, for pure p-GaAs at 300 K, the iterative calculation for the hole (drift) mobility of 371 cm^2/V s agrees well with the experimental value 400 cm^2/V s (Ref. 24) from Hall effect measurements.

Figure 3 compares the calculated mobility versus temperature of 4.5×10^{19} cm^{-3} Be-doped GaSb to experiment. The accuracy of the calculation improves with increasing temperature up to 450 K. This is possibly due to the fact that the Born approximation for ionized impurity scattering is more accurate at higher hole energies. Note the onset of substrate conduction beyond 450 K, as evidenced by the abrupt drop in mobility and eventual reversal in polarity of the Hall voltage around 550 K. Hence we do not have information on GaSb in that temperature regime.

Figure 4 shows the room-temperature Seebeck coefficient as a function of the hole concentration. Agreement to within 10% is observed between 1×10^{17} and 3×10^{19} cm^{-3}. In all cases, the Seebeck coefficient computed using five iterations for the BTE solution [$M=5$ in Eq. (9)] differs from the result of the noniterative computation by not more than 1%. For example, for $p=2.2\times10^{19}$ cm^{-3} at 700 K, the first few iterates for the Seebeck coefficient are 242.85, 241.41, 240.99, 240.88, and 240.85 μV/K. These differences cannot be resolved experimentally; thus setting $M=1$ in Eqs. (9a) and (9b), substituting in Eq. (10) for the current profile and equating to zero yields immediately the common procedure for determining the Seebeck coefficient of a two-band system;

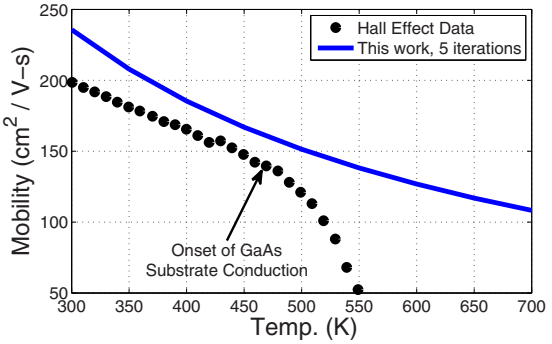

FIG. 3. (Color online) Hole mobility vs temperature: 4.5×10^{19} cm^{-3} Be-doped GaSb.

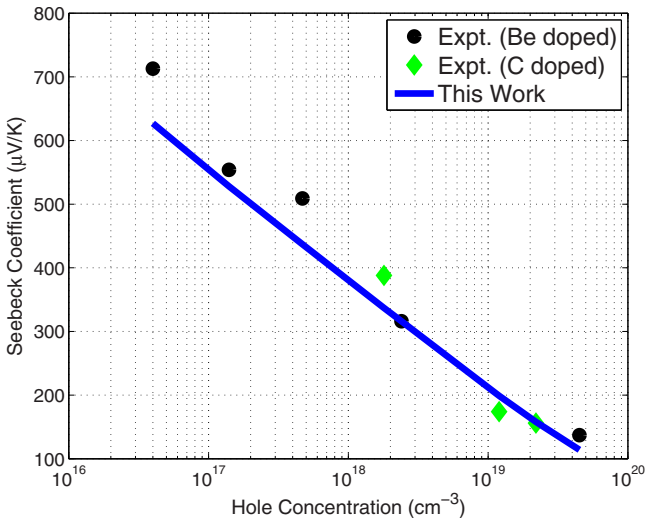

FIG. 4. (Color online) Room temperature Seebeck coefficient vs hole concentration (same series of GaSb films as in Fig. 2).

$$S=\frac{\sigma_i S_i+\sigma_j S_j}{\sigma_i+\sigma_j}, \tag{31a}$$

$$\sigma_n=\left(\frac{q^2}{3\pi^2\hbar}\right)\int_{k_n=0}^{\infty}\left(-\frac{\partial f_{0n}}{\partial k_n}\right)\tau_{n-\mathrm{eff}}(k_n)v_n(k_n)k_n^2dk_n$$

$$=\int_{k_n=0}^{\infty}\sigma_n(k_n)dk_n, \tag{31b}$$

$$S_n=-\frac{1}{qT}\left\{\frac{\int_{k_n=0}^{\infty}\sigma_n(k_n)[-E(k_n)+E_F-E_V]dk_n}{\int_{k_n=0}^{\infty}\sigma_n(k_n)dk_n}\right\}, \tag{31c}$$

where σ_n and S_n, $n=i,j$ are the conductivities and Seebeck coefficients of the individual bands.

For the UID sample with hole concentration 4×10^{16} cm^{-3}, the discrepancy between the calculated and measured values of the Seebeck coefficient (Fig. 4) is in part due to scattering by compensating donors, since for this sample, low temperature Hall effect data was fit very well by assuming a compensation ratio $N_D^+/N_A\sim1$. However compensation is ignored in all Seebeck coefficient and mobility calculations presented in this work since it necessitates the introduction of a fitting parameter, the compensation ratio.

VII. CONCLUSIONS

A formalism was developed for the semiclassical treatment of thermoelectric transport in p-type semiconductors whose valence band-structure can be described by two interacting bands. A procedure was described for extracting the Seebeck coefficient and mobility from this formalism. Convenient closed form expressions were written for intraband and interband scattering rates due to the four key scattering mechanisms. It was proved, using the typical III–V GaSb as an example that the usual artifice of combining the Seebeck coefficients as the weighted average of the individual band values, weighed by their respective conductivities, causes negligible error. For mobility calculation, it is seen that the iterative procedure of Eq. (11) with $M=5$ generally results in better agreement with experiment than the noniterative calculation; where it does not, it illustrates the limitations of the transition probability models.

ACKNOWLEDGMENTS

We are indebted to Dr. Emmanouil Kioupakis, Materials Dept., U.C. Santa Barbara for insightful suggestions during crucial stages of this project. The authors wish to thank Professor Ali Shakouri, Dr. Gehong Zeng, Dr. Je-Hyeong Bahk, Mr. Peter G. Burke, and Dr. Xiang Liu for several helpful discussions. This work was funded under the DARPA DSO Nanostructured Materials for Power Program (U.S. Army, W911NF08-1-0347).

[1] D. J. Howarth and E. H. Sondheimer, Proc. R. Soc. Lond. A Math. Phys. Sci. **219**, 53 (1953).
[2] D. L. Rode, Phys. Rev. B **2**, 1012 (1970).
[3] A. T. Ramu, L. E. Cassels, N. H. Hackman, H. Lu, J. M. O. Zide, and J. E. Bowers, J. Appl. Phys. **107**, 083707 (2010).
[4] E. O. Kane, J. Phys. Chem. Solids **1**, 249 (1957).
[5] K. Seeger, *Semiconductor Physics: An Introduction* (Springer-Verlag, Berlin, 1985).
[6] D. Kranzer, Phys. Status Solidi A **26**, 11 (1974).
[7] B. W. Kim and A. Majerfeld, J. Appl. Phys. **79**, 1939 (1996).
[8] B. Lax and J. G. Mavroides, Phys. Rev. **100**, 1650 (1955).
[9] J. M. Luttinger and W. Kohn, Phys. Rev. **97**, 869 (1955).
[10] M. Lundstrom, *Fundamentals of Carrier Transport*, 2nd ed. (Cambridge University Press, Cambridge, 2000).
[11] B. W. Kim and A. Majerfeld, Phys. Rev. B **51**, 1553 (1995).
[12] M. W. Heller and R. G. Hamerly, J. Appl. Phys. **57**, 4626 (1985).
[13] I. Vurgaftman, J. R. Meyer, and L. R. Ram-Mohan, J. Appl. Phys. **89**, 5815 (2001).
[14] D. V. Widder, *Advanced Calculus*, 2nd ed. (Prentice Hall, New Delhi, 2000).
[15] G. E. Pikus and G. L. Bir, Fiz. Tverd. Tela (Leningrad) **1**, 154 (1959).
[16] J. D. Wiley, Phys. Rev. B **4**, 2485 (1971).
[17] P. Lawaetz, Phys. Rev. B **174**, 867 (1968).
[18] D. L. Rode and S. Knight, Phys. Rev. B **3**, 2534 (1971).
[19] C. Kittel, *Introduction to Solid State Physics*, 7th ed. (Wiley, New York, 1996).
[20] G. L. Bir and G. E. Pikus, Fiz. Tverd. Tela (Leningrad) **2**, 2287 (1960).
[21] The NSM archive, Ioffe Institute. URL: http://www.ioffe.rssi.ru/SVA/NSM/Semicond/
[22] A. Subekti, V. W. L. Chin, and T. L. Tansley, Solid-State Electron. **39**, 329 (1996).
[23] A. R. Giehl, M. Kessler, A. Grosse, N. Herhammer, and H. Fouckhardt, J. Micromech. Microeng. **13**, 238 (2003).
[24] D. E. Hill, J. Appl. Phys. **41**, 1815 (1970).